Available online at www.sciencedirect.com
SCIENCE DIRECT®
Acta Materialia 52 (2004) 1003–1012
Acta MATERIALIA
www.actamat-journals.com

A texture optimization study for minimum earing in aluminium by use of a texture component crystal plasticity finite element method

Z. Zhao [a], W. Mao [b], F. Roters [c], D. Raabe [c,*]

[a] Department of Aeronautics and Astronautics, Massachusetts Institute of Technology, 77 Massachusetts Ave, Cambridge, MA 02139, USA
[b] Department of Materials Science and Engineering, University of Science and Technology Beijing, Beijing 100083, China
[c] Max-Planck-Institut für Eisenforschung, Max-Planck-Str. 1, 40237 Düsseldorf, Germany

Received 12 December 2002; accepted 6 March 2003

Abstract

The influence of discrete texture components and combinations of them on the earing behavior of aluminium during cup drawing was systematically investigated using the texture component crystal plasticity finite element method. Several common texture components and their combinations were selected and the resulting ear profiles were calculated under consideration of texture changes. The spherical scatter width of the components was also taken into account as an optimization parameter. The study reveals that the ear height and profile can be minimized by an optimized combination of certain texture components including their scatter width. A solution for minimum earing of cup drawn aluminium was obtained for a combination of the S and the Cube texture components with 15° spherical scatter width.

Keywords: Crystallographic texture; Deformation; Modeling; Earing; fcc; Aluminium

1. Motivation

Engineering polycrystalline materials often exhibit significant elastic–plastic anisotropy that can be attributed to the presence of crystallographic texture.

In the early industrial practice texture was long a property of polycrystals which was simply inherited from the preceding processing steps without conducting particular anisotropy optimization. This means that textures were known as an inevitable side-effect of materials processing which was hard to avoid and often accepted as it was. In contrast, modern industrial process design gradually aims at optimizing microstructures and properties during production, i.e., its goal consists in exploiting metallurgical mechanisms such as crystal plasticity, recrystallization, grain growth, and phase transformation for the design of well tailored crystallographic textures with respect to certain desired anisotropy properties of the final product.

A typical example is the development of $\{1\,1\,1\}\ \langle u\,v\,w\rangle$ textures of soft interstitial-free steels (IF steels) which are optimized with respect to sheet forming. In these body centered cubic (bcc) materials the $\{1\,1\,1\}\ \langle 1\,1\,\bar{2}\rangle$ and $\{1\,1\,1\}\ \langle 1\,\bar{1}\,0\rangle$ texture components each reveal a sixfold symmetry of the shape change with respect to the sheet surface, due to the symmetry of the active crystallographic slip dyads. In case that a complete fiber texture exists with a common $\langle 1\,1\,1\rangle$ crystal axis parallel to the sheet surface a very high planar-through-thickness anisotropy (r-value or Lankford-value) and a vanishing in-plane anisotropy (Δr-value) exists.

The most recent phase in the advancement of quantitative texture and anisotropy engineering consists in the introduction of inverse texture simulation methods. Such approaches are designed for the physically based tailoring of optimum textures for final products under consideration of prescribed processing and materials conditions on an inverse basis. This means that variational texture

* Corresponding author. Tel.: +49-211-6792278; fax: +49-211-6792333.
E-mail address: raabe@mpie.de (D. Raabe).

1359-6454/$30.00 © 2003 Acta Materialia Inc. Published by Elsevier Ltd. All rights reserved.
doi:10.1016/j.actamat.2003.03.001

optimization can nowadays be conducted in a way to match some desired final anisotropy and can help to identify beneficial corresponding processing parameters. This amounts to a tenet change in the sense that the process should no longer determine the textures but the desired textures should determine the process.

Plastic anisotropy during deep drawing may entail the formation of uneven rims of the drawn product, usually referred to as *earing*. One important consequence of that is – besides the irregular shape of the drawn specimen – an inhomogeneous distribution of the mechanical properties and of the wall thickness due to volume conservation and the kinematically necessary strain rate variation.

The trivial solution for the control and minimization of earing would be the presence of a random crystallographic texture prior to loading. However, such a supposed obvious approach is prevented due to two reasons. First, random *starting* textures do generally not remain random when the material is plastically deformed. This applies in particular to sheet forming operations. Second, complete spherical and topological randomization of textures is very difficult. Most metallurgical and mechanical processes promote rather reduce orientation distributions. This applies in particular to most face centered cubic (fcc) metals, in particular to those without bulk phase transformation during forming such as aluminium.

Therefore, a more practical approach for reducing shape anisotropy lies in combining the texture components constituting the initial sheet in such a way that the resulting ear profile – accounting also for texture changes *during* forming – can be minimized owing to the mutual compensation of the shape anisotropy contributions introduced by the individual texture components during forming.

The present work pursues this approach. We apply an inverse texture simulation method to the optimization of the shape anisotropy occurring during cup drawing of fcc polycrystals with a high stacking fault energy containing a large number of grains (large meaning $n_{\text{grains}} > 10^4$ as typically present in engineering sheet material). As a typical sample material we choose the constitutive behavior of aluminium. The rolling texture in such alloys is primarily composed of the S orientation, $\{1\,2\,3\}\ \langle 6\,3\,\bar{4}\rangle$, the Brass orientation, $\{1\,1\,0\}\ \langle 1\,\bar{1}\,2\rangle$, and the Copper orientation $\{1\,1\,2\}\ \langle 1\,1\,\bar{1}\rangle$. These texture components promote earing essentially at 45°/135° with respect to the rolling direction. Annealing textures which may contain the Cube orientation, $\{1\,0\,0\}\ \langle 0\,0\,1\rangle$, and also some Goss orientation, $\{1\,1\,0\}\ \langle 0\,0\,1\rangle$, also promote pronounced earing, namely, at the 0/90° directions for the Cube orientation and the Goss orientation [1–9]. A useful approach, therefore, might consist in creating a sheet material with a low ear ratio by a suitable combination of crystals with an orientation that results in 45°/135° ears and those that produce 0/90° ears [1,2].

In order to identify a theoretical solution for minimum shape anisotropy after deep drawing as a result of a suited combination of these orientations we employ a texture component crystal plasticity finite element method [10–14]. The use of this new simulation method offers five main advantages. First, the approach allows one to conduct predictions of earing including all texture changes occurring during deep drawing. Second, the method is quantitative. Third, the approach allows us to also simulate wall thickness and heterogeneity of the mechanical properties after deformation. Fourth, the predictions include the optimization of the spherical scatter width of texture components. Fifth, the methods allows us to directly feed in the starting textures.

The purpose of this paper consists first, in deriving the ideal texture composition for minimum earing in fcc metals with high stacking fault energy in a quantitative fashion and second, to establish the texture component crystal plasticity finite element method as a pertinent inverse materials engineering tool for anisotropy optimization.

After an introduction to the new texture component crystal plasticity finite element method (TCCP-FEM) and to the model set-up we simulate the individual ear profiles of some main texture components of rolled and annealed aluminum. Subsequently, we present for two of them, namely, for the Cube and the S orientation, a set of simulations which aims at optimizing their volume ratio for obtaining minimum earing including the discussion of the influence of the spherical scatter width of the texture components on the ear profile.

2. The texture component crystal plasticity finite element method

2.1. Basics

Crystal plasticity finite element models represent helpful tools for detailed simulation studies of texture evolution under realistic mechanical boundary conditions and under consideration of texture update. A direct implementation of crystal plasticity theory into finite element models was first suggested by Pierce and coworkers [15–18]. Based on their work a fully-implicit time-integration scheme was developed by Kalidindi et al. [19] and implemented in commercial finite element software. This model provides a direct means for updating the material state via integration of the evolution equations for the crystal lattice orientation and the critical resolved shear stresses of the individual slip systems.

An intrinsic challenge of directly integrating constitutive polycrystal plasticity laws into finite element approaches lies in identifying an effective method of mapping a *representative* crystallographic texture, com-

prising a *large* number of grains, on the integration points of the finite element mesh using a compact mathematical form which still permits texture update during loading.

It is an essential boundary condition in this context that crystal plasticity finite element approaches require a *discrete* representation of the orientation distribution function at each integration point. When dealing with a relatively small number of grains (small meaning $n_{\text{grains}} < 10^4$) a discrete mapping of the texture is achieved by a simple one-to-one approach, where each Gauss point in the finite element mesh is occupied by one discrete crystallographic orientation. This approach, however, is inappropriate when simulating samples which contain a much larger number of grains. From an engineering perspective it is obvious that an appropriate mapping of such a discrete texture requires the reduction of the orientational information content to a level at which complex deformation processes can be simulated without the help of a supercomputer.

2.2. Texture components

The texture component method offers a useful approach in the context described above. It is a technique of approximating the orientation distribution function in the form of discrete sets of symmetrical spherical model functions which are defined in orientation space. The model functions have individual height and individual full width at half maximum as a measure for the strength and scatter of the crystallographic texture component they represent. They are typically formulated as central functions which have an isotropic scatter in orientation space.

The mathematical reproduction of the orientation distribution function by texture component functions can be expressed by the superposition

$$f(g) = F + \sum_{c=1}^{C} I^c f^c(g) = \sum_{c=0}^{C} I^c f^c(g) \quad \text{where } I^0 = f, \quad f^0(g) = 1, \tag{1}$$

where g is the orientation, $f(g)$ is the orientation distribution function, and F is the volume portion of all randomly oriented crystals (random texture component). F may be understood as the intensity of the only *global* component used in the approximation, equivalent to $f^c(g) = 1$ for each orientation point in Euler space, $g \in G$. The intensity I^c describes the volume fraction of all crystallites belonging to the component c. The orientation density of the component is described by a central function, i.e., its value decreases isotropically with increasing orientation distance $\tilde{\omega}^c = \tilde{\omega}(g^c, g)$ from the maximum. This means that $f^c(g)$ only depends on $\tilde{\omega}^c = \tilde{\omega}(g^c, g)$, but it is independent on the rotation axis $\tilde{n}^c$.

The orientation distribution function is defined by

$$f(g)\mathrm{d}g = 8\pi^2 \frac{\mathrm{d}V_g}{V} \quad \text{which implies } f(g) \geqslant 0, \tag{2}$$

where V is the sample volume and $\mathrm{d}V_g$ the volume of all crystals with an orientation g within the orientation portion $\mathrm{d}g = sin(\phi)\mathrm{d}\phi\,\mathrm{d}\varphi_1\,\mathrm{d}\varphi_2$. Normalization requires

$$\oint f^c(g)\,\mathrm{d}g = 1 \quad \text{which implies } \sum_{c=0}^{C} I^c = 1. \tag{3}$$

As a rule texture components require positivity, i.e.,

$$f^c(g) \geqslant 0 \quad \text{for all } g \in G \quad \text{and} \quad I^c > 0, \tag{4}$$

where G is the orientation space.

Spherical central functions, including corresponding pole figures, can generally be represented in the form of series expansions of χ functions or, respectively, Legendre polynomials. More practical approximations of texture components have been introduced on the basis of spherical Gauss- and Lorentz-functions. The work presented in this study makes use of Gauss-shaped model functions for the decomposition of the orientation distribution function which are described by

$$f^c(g) = N^c \exp\left(S^c \cos\tilde{\omega}\right), \tag{5}$$

where

$$S^c = \frac{\ln 2}{1 - \cos(b^c/2)} \quad \text{and} \quad N^c = \frac{1}{I_0(S^c) - I_1(S^c)}. \tag{6}$$

The according pole figure projections $P_h^M(g^c, b^c, y)$ can be calculated in closed analytical form

$$P_h^M(g^c, b^c, y) = N^c \exp\left(S^c \sin(\upsilon^c/2)\right) I_0(S^c \cos(\upsilon^c/2)), \tag{7}$$

where υ^c describes the geometry of the component in the respective pole figure projection and $I_l(x)$ are generalized Bessel functions. The value b^c is the halfwidth and can be interpreted as the mean diameter of a spherical component in orientation space and g^c is the center orientation of the texture component [22].

The components describing $f(g)$ can be determined by the best fit of the experimental pole figure input data $\tilde{P}_{h_i}^M(y_r)/N_{h_i}$ with the recalculated pole figures $\sum_c I^c \tilde{P}_h^M(g^c, b^c, y_r)$. The index r marks the measured sample directions y_r. The component parameters I^c, g^c and b^c and the normalization N_{h_i} of the pole figures are obtained by solving the least squares problem

$$\sum_{i,r} w_{ir} \left[\tilde{P}_{h_i}(y_r)/N_{h_i} - \sum_c I^c \tilde{P}_{h_i}^M(g^c, b^c, y_r)\right]^2 \Rightarrow \text{Min}, \tag{8}$$

where w_{ir} are weight factors. Usually the parameters g^c and b^c must be calculated by a non-linear algorithm. First estimates are required, which may be obtained manually from the graphical representation of the difference pole figures which are calculated according to

$$\Delta_{h_i}(y_r) = \tilde{P}_{h_i}(y_r) - \sum_c I^c \tilde{P}^M_{h_i}(g^c, b^c, y_r). \quad (9)$$

Depending on experience in interpreting crystallographic textures the user can specify the position, height, and scatter of the texture components within certain bounds before the minimization. This makes particularly good sense when the number of texture components initially prescribed to match an experimental texture is small or when a certain scatter width of the components should not be exceeded.

In contrast to the use of global symmetric Wigner functions as used for instance in the Fourier-type series expansion methods, the texture component method is well suited for an incorporation of texture into crystallographic finite element methods. This advantage is due to the fact that the method is based on using sets of localized spherical normalized standard functions which are characterized by simple parameters of physical significance (Euler angle triple for the main orientations, volume fractions, full widths at half maximum). Typically only a few texture components are required to describe the orientation distribution function which in turn can represent the texture of any grain assembly whatever size it may have. The texture component method allows one to extract texture information in a compact fashion from experiment or theory.

The texture component method was originally introduced by Lücke et al. [20,21] and later improved by Helming [22]. The basic idea of using texture components, however, goes back to the early texture studies where experimental and predicted pole figures were mostly interpreted in terms of the evolution and physical significance of discrete texture components. Classical terms introduced in these early studies on crystallographic orientation distributions were for instance the "Copper texture component", the "Brass texture component", or the "Taylor texture component" (the stable orientation of a Taylor Full Constraints model). The use of preferred orientations prevailed in texture research until the late sixties of the last century, i.e., statements about texture evolution were made practically exclusively on the basis of pole figures and estimated preferred components (ideal positions, texture components).

In Section 2.4 we will describe how texture components can be decomposed and mapped on a finite element grid in cases where the underlying constitutive model has been formulated in an orientation dependent fashion.

2.3. The crystal plasticity constitutive model

In our approach we use the large-strain constitutive crystal plasticity model suggested by Kalidindi [19]. In this formulation one assumes the stress response at each macroscopic continuum material point to be potentially given by one crystal or by a volume-averaged response of a set of grains comprising the respective material point. The latter assumption can be referred to as a local Taylor-type or local strain-rate homogenization assumption. In case of a multi-grain description the volume averaged stress amounts to

$$\langle \mathbf{T} \rangle = \sum_{k=1}^{N} (w_k \mathbf{T}_k), \quad (10)$$

where N is the total number of individual orientations mapped onto an integration point using the Taylor assumption, w_k the volume fraction of each single orientation extracted from a texture component as described above, $\mathbf{T}_k$ the Cauchy stress produced by the kth individual orientation, and $\langle \mathbf{T} \rangle$ the volume average stress produced by all orientation mapped at the integration point. The constitutive equation for the stress in each grain is then expressed in terms of

$$\mathbf{T}^* = \mathbf{C}\mathbf{E}^*, \quad (11)$$

where $\mathbf{C}$ is the fourth order elastic tensor and $\mathbf{E}^*$ an elastic strain measure,

$$\mathbf{E}^* = \tfrac{1}{2}\left(\mathbf{F}^{*\mathrm{T}}\mathbf{F}^* - 1\right) \quad (12)$$

obtained by the polar decomposition,

$$\mathbf{F} = \mathbf{F}^* \mathbf{F}^{\mathrm{p}}, \quad (13)$$

which leads to a stress measure which is the elastic work conjugate to the strain measure $\mathbf{E}^*$,

$$\mathbf{T}^* = \mathbf{F}^{*-1}(\det(\mathbf{F}^*)\mathbf{T})(\mathbf{F}^*)^{-\mathrm{T}}, \quad (14)$$

where $\mathbf{T}$ is the symmetric Cauchy stress tensor in the grain, and $\mathbf{F}^*$ is a local elastic deformation gradient defined in terms of the local *total* deformation gradient $\mathbf{F}$ and the local *plastic* deformation gradient $\mathbf{F}^{\mathrm{p}}$. According to Eq. (12) the relation between the elastic and the plastic portion of $\mathbf{F}$ amounts to

$$\mathbf{F}^* = \mathbf{F}(\mathbf{F}^{\mathrm{p}})^{-1}, \quad \det(\mathbf{F}^*) > 0, \quad \det(\mathbf{F}^{\mathrm{p}}) = 1. \quad (15)$$

The plastic deformation gradient is given by the flow rule

$$\dot{\mathbf{F}}^{\mathrm{p}} = \mathbf{L}^{\mathrm{p}}\mathbf{F}^{\mathrm{p}} \quad (16)$$

with its crystalline portion

$$\mathbf{L}^{\mathrm{p}} = \sum_{k=1}^{N} \dot{\gamma}_k m_k, \quad m_k = \hat{b}_k \otimes \hat{n}_k, \quad (17)$$

where m_k are the kth dyadic slip products of unit vectors $\hat{b}_k$ in the slip direction and $\hat{n}_k$ normal to the slip plane, and $\dot{\gamma}_k$ the shear rates on these systems. The specific constitutive functions for the plastic shearing rates $\dot{\gamma}_k$ on the slip systems are taken as

$$\dot{\gamma}_k = \dot{\gamma}_o \left| \frac{\tau_k}{\tau_{k,\mathrm{crit}}} \right|^{1/m} \mathrm{sgn}(\tau_k), \quad (18)$$

where τ_k is the resolved shear stress for the slip system k, and $\tau_{k,\mathrm{crit}}$ is the actual critical shear stress on the kth slip system. $\dot{\gamma}_o$ and m are material parameters representing shearing rate and the rate sensitivity of slip. The calculation of $\tau_{k,\mathrm{crit}}$ has been achieved by accounting for latent hardening through the use of an appropriate hardening matrix,

$$\dot{\tau}_{k,\mathrm{crit}} = \sum_i h^{ki}\left|\dot{\gamma}^i\right|, \quad h^{ki} = q^{ki}h^{(i)}, \tag{19}$$

where h^{ki} is the rate of strain hardening on kth slip system due to a shearing on ith slip system, q^{ki} is the hardening matrix describing the latent hardening behavior of a crystallite, and $h^{(i)}$ is the hardening rate of the single slip system i. In the present study, 12 slip systems with crystallographic $\langle 1\,1\,0\rangle$ slip directions and $\{1\,1\,1\}$ slip planes are taken into account for room temperature simulations of plastic deformation of aluminium. The matrix h^{ki} can be taken as

$$h^{ki} = \begin{bmatrix} A & qA & qA & qA \\ qA & A & qA & qA \\ qA & qA & A & qA \\ qA & qA & qA & A \end{bmatrix}, \tag{20}$$

where q is the ratio of the latent hardening rate to the self-hardening rate, and A is a 3×3 matrix populated by ones. Using this constitutive description renders the finite element method an elegant tool for detailed simulation studies of texture evolution and strain distribution under realistic boundary conditions. Each integration point can represent one single orientation or a larger set of crystals as outlined above [9–14].

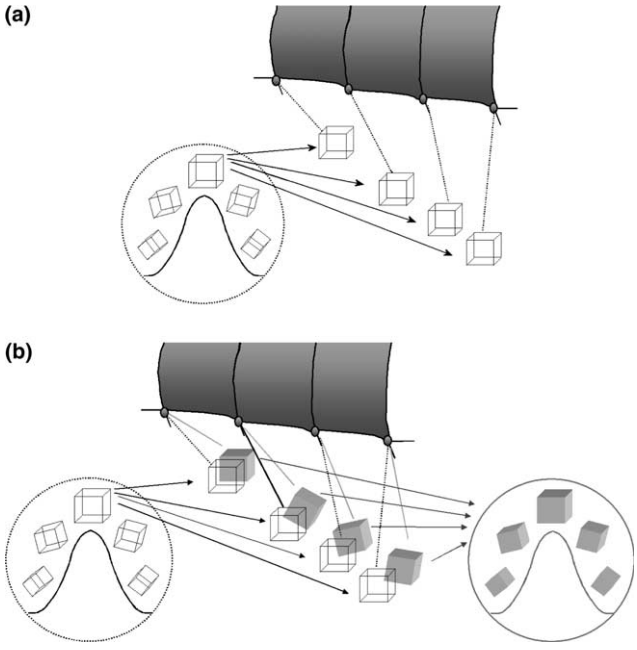

Fig. 1. (a) Schematic drawing showing the first step of the decomposition of a texture component where the preferred orientation (center or mean orientation of the texture component) is extracted from the texture component and assigned in terms of its respective Euler triple $(\varphi_1, \phi, \varphi_2)$, i.e., in the form of a single identical rotation matrix, onto each integration point. In this state the sample is a single crystal. (b) Schematic drawing showing the second step of the decomposition of a texture component where the mapped single orientations taken from the center of the texture component are systematically rotated in such a fashion that their resulting overall distribution reproduces exactly the original texture function which was prescribed in the form of a texture component.

2.4. Using texture components in a crystal plasticity finite element simulation

The main task of the new concept is to represent sets of spherical Gaussian texture components on the integration points of a finite element mesh for a crystal plasticity simulation. This procedure works in two steps: First, the discrete preferred orientation g^c (center orientation, mean orientation) is extracted from each of the texture components and assigned in terms of its respective Euler triple $(\varphi_1, \phi, \varphi_2)$, i.e., in the form of a *single* rotation matrix, onto *each* integration point (Fig. 1(a)). For this step we use the method of Helming [22]. In the second step, these discrete orientations are re-oriented in such a fashion that their resulting overall distribution reproduces the texture function which was originally prescribed in the form of a Gaussian texture component (Fig. 1(b)). In other words the orientation scatter described initially by a texture component function is in the finite element mesh represented by a systematically re-oriented set of orientations, each assigned to one integration point, which reproduces the original spherical scatter prescribed by that component. This means that the scatter which was originally only given in orientation space is now represented by a distribution both, in real space and in orientation space, i.e., the initial spherical distribution is transformed into a spherical *and* lateral distribution. The described allocation and re-orientation procedure is formulated as a weighted sampling Monte Carlo integration scheme in Euler space. It is important in this context, that the use of the Taylor assumption locally allows one to map more than one preferred crystallographic orientation on each integration point and to assign to each of them an individual volume fraction (Fig. 2). This means that the procedure of mapping and rotating single orientations in accord with the initial texture component scatter width is individually conducted for *all* prescribed components as well as for the random background extracted from initial experimental or theoretical data.

After decomposing and representing the initial texture components as a lateral and spherical single orientation distribution in the mesh, the texture component concept is no longer required in the further procedure. This is due to the fact that during the subsequent crystal plasticity finite element simulation each individual

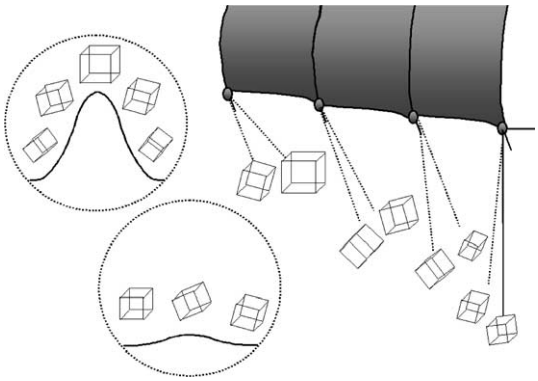

Fig. 2. Schematic drawing showing the mapping of different texture components on a mesh.

orientation originally pertaining to one of the texture components can undergo an *individual* orientation change as in the conventional crystal plasticity methods. This means that the texture component method loses its significance during the simulation. In order to avoid confusion one should, therefore, underline that the texture component method is used to *feed* textures into finite element simulations on a strict physical and quantitative basis. The components as such, however, are in their original form as compact functions not tracked during the simulation. It must also be noted that the orientation points which were originally obtained from the components do not represent individual *grains* but portions of an orientation distribution function.

3. Set-up of the finite element model and simulation details

The finite element calculations were carried out using the commercial finite element program ABAQUS in conjunction with the user defined material subroutine UMAT [23]. An implicit crystal plasticity procedure developed by Kalidindi [19] was implemented and used for the time integration of the constitutive equations. Hardening was fitted to match the behavior of pure aluminium. We used the 12 $\{1\,1\,1\}\ \langle 1\,\bar{1}\,0\rangle$ slip systems to formulate the crystallographic slip dyads.

Fig. 3(a) shows the geometry of the tools used in the simulation. Due to the orthotropic sample symmetry, only a quarter of the blank has to be represented in the simulation. Fig. 3(b) shows the mesh configuration of the specimen prior to loading. The angular element density increases from the blank center to the border in order to obtain good accuracy along the final border of the cup. The blank was modeled using 432 elements of type C3D8 and 80 elements of type C3D6.

The interaction between the blank and the blank holder was modeled in three steps. In the first step the blank holder was pushed onto the blank with a prescribed displacement corresponding to zero clearance across the interface between the blank and the holder. A specified clamping pressure was imposed across the element thickness via softened surface control. In the present simulations we used an exponential soft contact function. In the second step, the blank holder was fixed in its current positions. This two-step procedure created contact between the blank holder and the blank. In the final step the punch was moved toward the blank through a total distance of 80 mm. This step modeled the actual drawing process.

Considering that this paper is mainly focused on the theoretical analysis of the relationship between texture components and earing behavior rather than on the comparison of the difference between simulation and experimental results, the Coulomb friction coefficient was assumed as $\mu = 0$ to reduce computing time. In various previous articles [10–12,24,25] where we had studied the influence of different friction conditions ($\mu = 0$–0.2) on the simulation results we repeatedly

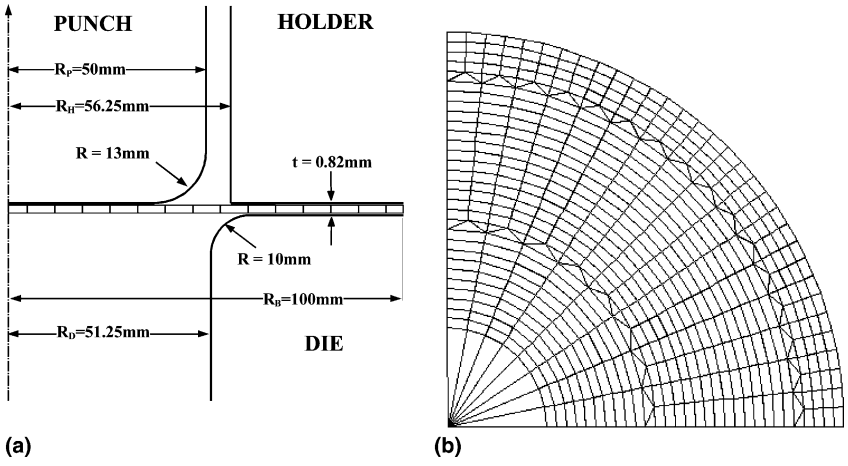

Fig. 3. (a) Finite element model set-up showing the geometry of the tools used in the simulations (mm as arbitrary units). (b) Mesh configuration. For considering the orthotropic symmetry, only a quarter of the blank is employed which is modeled using 432 elements of type C3D8 and 80 elements of type C3D6. The angular element number increases from the center to the border in order to reach a sufficient accuracy along the rim of the cup.

found that changes of the friction coefficient had only little influence on the *relative* ear height. We attributed this observation to the fact that – different than in classical J2 continuum simulations – nonuniform deformation and strain localization naturally arise in polycrystals as a consequence of crystallographic slip. Similar observations were earlier reported by Dève et al. [26] and Harren and Asaro [27].

In this study, we use a set of well known *ideal* texture components with a set of given Euler angles as a basis, namely, Cube ($\varphi_1 = 0°$, $\phi = 0°$, $\varphi_2 = 0°$), S ($\varphi_1 = 60°$, $\phi = 32°$, $\varphi_2 = 65°$), Brass ($\varphi_1 = 35°$, $\phi = 40°$, $\varphi_2 = 0°$), Copper ($\varphi_1 = 90°$, $\phi = 30°$, $\varphi_2 = 45°$), and Goss ($\varphi_1 = 0°$, $\phi = 45°$, $\varphi_2 = 0°$). The plasticity simulations are then conducted with different combinations of them in terms of their individual volume fraction and spherical scatter width.

In a first set of simulations the individual ear profiles were calculated separately for each of these components. Owing to the orthorhombic sample symmetry each single orientation has to be balanced by three additional symmetrically equivalent orientations in order to correctly reproduce the response of the material in the crystal plasticity finite element calculations. Consequently, each of the symmetrical variants was assigned one quarter of the volume of the original component. For the Cube and Goss orientations the crystallographic symmetry of these components with respect to the starting sample coordinates reduces the required initial equivalent variants to one and for the Copper component to two.

In a second set of simulations the Cube and S components were combined with the aim to reduce the ear height of the drawn cup. The two components were selected because they produce opposite earing and because they are typical texture components in fcc metals with high stacking fault energy [1–9,28,29]. We computed the ear profiles of the different combinations as a function of their volume fractions and spherical scatter widths. The aim of this simulation series is the prediction of the optimum texture composition for minimum earing. Earing is quantified in terms of the ear height and ear area (Fig. 4). The ear height describes the difference between the highest point on the rim and the lowest point on the profile of the drawn cup. The ear area integrates the entire surface above the lowest point on the rim.

In both simulation series the ear profiles were calculated with different values for the full width at half maximum of the underlying spherical Gauss functions ranging from 5° to 15°.

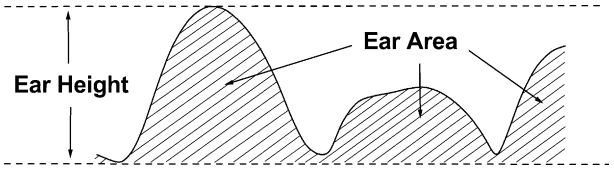

Fig. 4. Earing is quantified in terms of the ear height and the ear area. The ear height describes the difference between the highest point on the rim and the lowest point on the profile of the drawn cup. The ear area integrates the entire surface above the lowest point on the rim.

4. Results and discussion

4.1. Ear profiles of individual texture components

Fig. 5 shows the simulated ear profiles of the five single texture components Cube, S, Brass, Copper, and Goss. The simulations were conducted for perfect single crystalline starting material, i.e., under the assumption of 0° scatter about the main orientations prior to loading. It must be underlined, though, that considerable orientation scatter is generated during deformation, i.e., the specimens do not remain single crystalline. The use of *mm* as a unit for the ear height is arbitrary like in all finite element simulations and only scaled by the units used for the description of the tool design (see Fig. 3(a)).

The ear shape of the Cube component reveals maximum ear height at the rolling and transverse directions

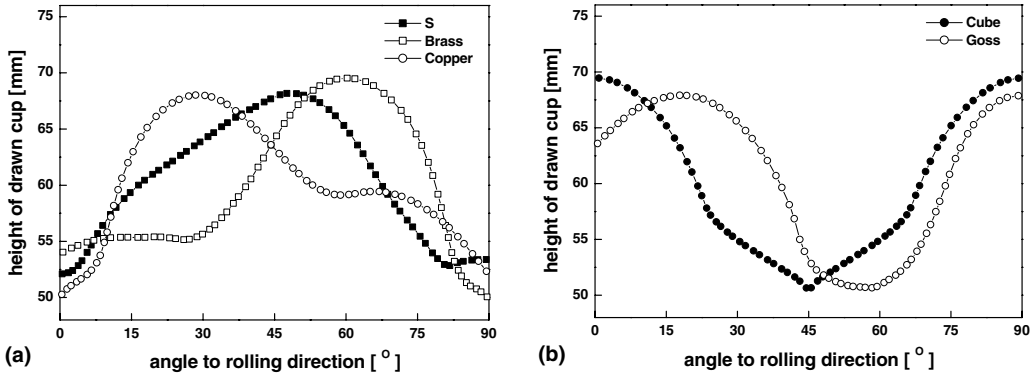

Fig. 5. Ear profiles of individual texture components. Five texture components are selected and their final ear profiles can be grouped into two types (a) 45°/135° type, such as S, Brass and Copper whose main ear peaks appear near 45° and 135° to the rolling direction, and (b) 0°/90° type, such as Cube and Goss, whose ear peaks appear near the rolling and transverse directions.

with an ideal orthotropic symmetry. Compared to this ear shape the maximum ear positions created by the Goss texture component are shifted about 15° away from those caused by the Cube single crystal towards the transverse direction. In contrast to the Cube and Goss orientations, the ear peaks of the S, Brass, and Copper texture components appear at about 45°, 60°, and 30° to the rolling direction, respectively. These predictions are in accordance with earlier findings of ear shapes made by other authors [1–9].

According to these data the five texture components can be grouped into two types according to the shape anisotropy after cup drawing, namely, into the 0°/90° type (Cube and Goss) and the 45°/135° type (S, Brass and Copper). The earing behavior between these two groups of texture components is opposite which means that earing minimization can be most likely achieved by mixing them in a reasonable fashion.

4.2. Earing minimization by combining texture components

Figs. 6(a) and (b) show the influence of a mixture of the S and the Cube texture components on the ear shape after cup drawing. The simulation results present the ear profiles for different ratios of the volume fractions of the two texture components. Fig. 6(a) shows that an optimum profile is obtained for a combination of 62.75 vol% of the S component and 37.25 vol% of the Cube component in case that the orientational scatter width amounts to 0° prior to elastic–plastic loading (combination of two originally perfect single crystals). Fig. 6(b) reveals that this results applies for both, the ear height and the ear area. Fig. 6(b) also demonstrates that the dependence of earing in terms of height and area on the texture composition reveals a steep change in the vicinity of the earing minimum, i.e., small modifications in the ratio of the volumes of the two texture components entail a strong change in earing. This means that even minor texture changes can lead to a remarkable optimization or degradation of the ear profile. It is important to note in this context that the *ideal* components with 0° orientational scatter width, which characterize the starting texture, develop during the simulation into an array of similar orientations, each of which may undergo individual reorientations according to the local boundary conditions. It is the special advantage of the texture component crystal plasticity finite element method to take these individual local reorientation- and strain-paths properly into account.

Fig. 7 illustrates the ear profiles and the geometry of the samples initially equipped with a Cube component (Fig. 7(a)), S component (Fig. 7(b)), and their optimum combination (Fig. 7(c)) during cup drawing. It is obvious that the rim of the sample initially designed with a combination of 62.75 vol% of the S component and 37.25 vol% of the Cube component reveals a much smoother shape when compared to the results obtained for the single crystals.

It is of some interest in this context to observe that the optimum volume ratio between the S orientation and the Cube orientation amounts to about 1.67:1 (62.75 vol%:37.25 vol%) rather than to 1:1. The reason for an initial assumption that an optimum ratio between the two texture components might amount to 1:1 was suggested by Fig. 5 which shows that the ear profiles created by the S and the Cube components are opposite indicating the possibility of mutual compensation. The fact that 1.67:1 and not 1:1 is the optimum ratio underlines that the interaction of different texture components is highly non-linear. It is also important to learn from this ratio that the volume fraction of the S component must obviously be much larger than that of the Cube component in order to compensate for anisotropy.

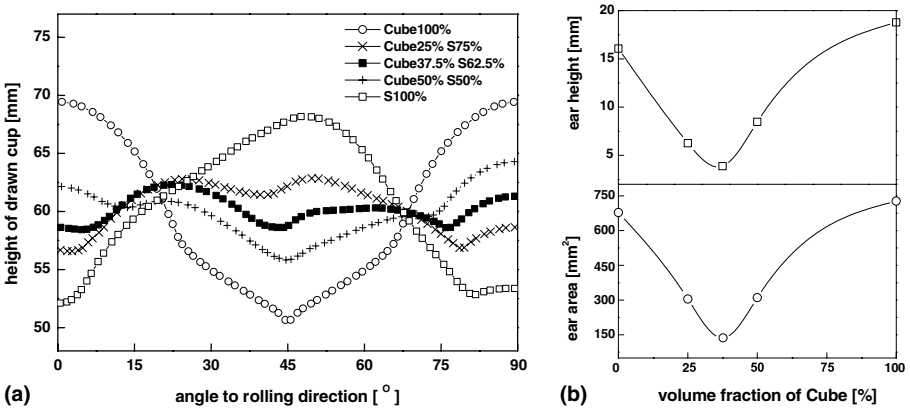

Fig. 6. Minimization of ear formation by mixing the S and Cube texture components. (a) Ear profiles for different ratios of S and Cube. (b) Quantitative analysis of ear height and ear area. The simulation results show that the ear behavior can be minimized by mixing S and Cube texture components at an optimum ratio of about 62.75 vol%/37.25 vol% (S/Cube). (a) Ear profiles (b) Quantitative analysis.

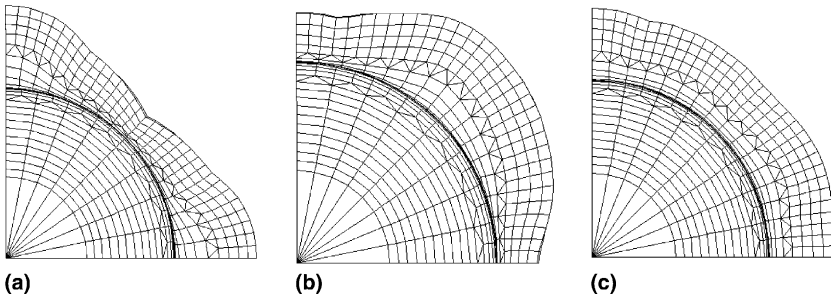

Fig. 7. Ear profiles during simulated cup drawing for discrete texture components (a) Cube, (b) S, (c) mixture of 37.25 vol% Cube and 62.75 vol% S.

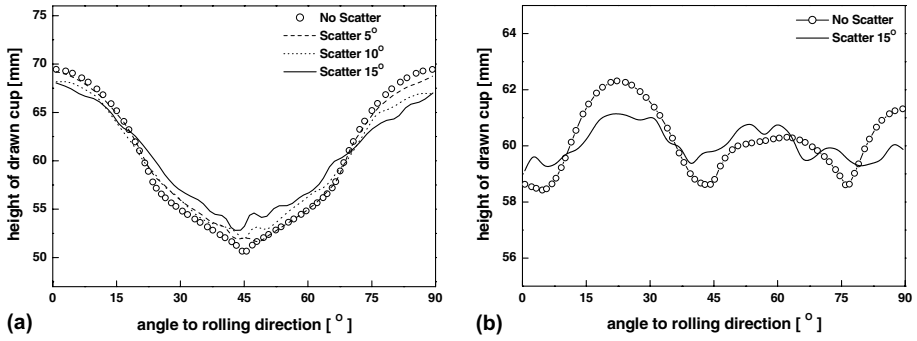

Fig. 8. Influence of the spherical full width at half maximum of the texture components on the ear profiles.(a) Cube component, (b) Cup containing 62.75 vol% S and 37.25 vol% Cube (with 0° and 15° spherical scatter (full width at half maximum)).

This means that the Cube orientation has a much larger effect on the overall anisotropy during deep drawing than the S orientation.

4.3. Effect of the spherical scatter width on the ear profiles

Fig. 8 shows the effects of the initial spherical scatter width of the texture components on the final ear profiles. Fig. 8(a) reveals for the Cube texture component that an increase in the initial orientation scatter from 0° to 15° results in a decrease in the ear height from 19 to 14 mm. Fig. 8(b) shows the result obtained for an increase in the initial orientation scatter for a combination of the Cube and the S components. Increasing the orientation scatter from 0° to 15° entails a substantial drop in the roughness of the rim after drawing (see also Fig. 9).

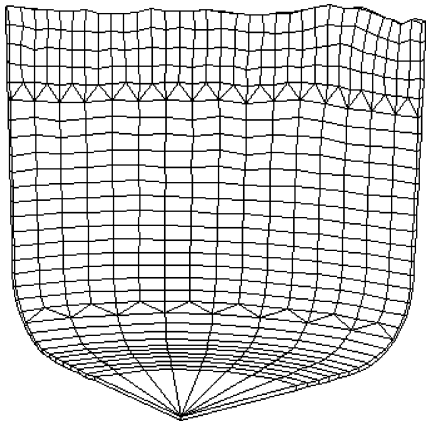

Fig. 9. Simulated quarter cup after drawing using 37.25 vol% Cube and 62.75 vol% S each with 15° spherical scatter (full width at half maximum).

5. Conclusions

We used a texture component crystal plasticity finite element method to investigate the influence of various texture components and their combination on the earing behavior of cup drawn aluminium samples. The following conclusions can be drawn from this study:

1. Ear peaks of the Cube and Goss texture components appear at the rolling and transverse directions, while the ears of the Copper, S and Brass orientations occur at about 45° and 135° to the rolling direction.
2. Minimization of earing can be achieved by mixing the Cube and S texture components. The optimum volume ratio between the two is S:Cube = 1.67:1.
3. Optimization of earing depends on both, crystallographic orientation and scatter width of the orientation components. As a rule earing decreases with increasing spherical scatter width of the texture components.

References

[1] Rollett AD, Canova GR, Kocks UF. In: Sachdev AK, Embury JD, editors. Proceedings of a TMS symposium on Metal Formability and Microstructure. Warrendale: TMS-AIME; 1986. p. 147.
[2] Morris J. Scr Metall Mater 1994;31:387.
[3] Daaland O, Nes E. Acta Mater 1996;44:1389.
[4] Savoie J, Zhou Y, Jonas JJ, MacEwen SR. Acta Metall 1996;44:587.
[5] Hu JG, Jonas JJ, Ishikawa T. Mater Sci Eng A 1998;256:51.
[6] Cheng XM, Liu Y, Morris JG. Aluminum Trans 1999;1:103.
[7] Inal K, Wu PD, Neale KW. Int J Plast 2000;16:635.
[8] Yoon JW, Barlat F, Chun K, Pourboghrat F, Yang DY. Int J Plast 2000;16:1075.
[9] Cheng XM, Morris JG. Mater Sci Eng A 2002;323:32.
[10] Zhao Z, Roters F, Mao W, Raabe D. Adv Eng Mater 2001; 3:984.
[11] Raabe D, Zhao Z, Roters F. Steel Res 2001;72:421.
[12] Raabe D, Roters F, Int J Plast 2004;20, in press.
[13] Raabe D, Roters F, Zhao Z. In Proceedings of the 8th International Conference on Aluminium Alloys in Cambridge, UK, July 2–5, 2002, Materials Science Forum, 2002;31:396–402.
[14] Raabe D, Helming K, Roters F, Zhao Z, Hirsch J. In Proceedings of the 13th International Conference on Textures of Materials ICOTOM 13, 2002, Seoul, Korea, Trans Tech Publications, Ed.: Dong Nyung Lee, Materials Science Forum, 2002;257:408–12.
[15] Pierce D, Asaro RJ, Needleman A. Acta Metall 1982;30:1087.
[16] Asaro RJ. Adv Appl Mech 1983;23:1.
[17] Pierce D, Asaro RJ, Needleman A. Acta Metall 1983;31:1951.
[18] Needleman A, Asaro RJ. Acta Metall 1985;33:923.
[19] Kalidindi SR, Bronkhorst CA, Anand L. J Mech Phys Solids 1992;40:537.
[20] Lücke K, Pospiech J, Virnich KH, Jura J. Acta Metall 1980;29:167.
[21] Lücke K, Pospiech J, Jura J, Hirsch J. Z Metallkunde 1986;77: 312.
[22] Helming K, Schwarzer RA, Rauschenbach B, Geier S, Leiss B, Wenk H, Ullemeier K, Heinitz J. Z Metallkd 1994;85:545.
[23] ABAQUS/Standard User's Manual, vol. 2, 14.1.4-1, Hibbitt, Karlsson, Sorensen, Pawtucket, RI, 1999.
[24] Raabe D, Sachtleber M, Zhao Z, Roters F, Zaefferer S. Acta Mater 2001;49:3433.
[25] Sachtleber M, Zhao Z, Raabe D. Mater Sci Eng A 2002;336:81.
[26] Dève H, Harren SV, McCullough C, Asaro RJ. Acta Metall 1988;36:341.
[27] Harren SV, Asaro RJ. J Mech Phys Solids 1989;37:191.
[28] Hirsch J, Lücke K. Acta Met 1988;36:2863.
[29] Engler O, Hirsch J. Mater Sci Eng A 2002;336:249.